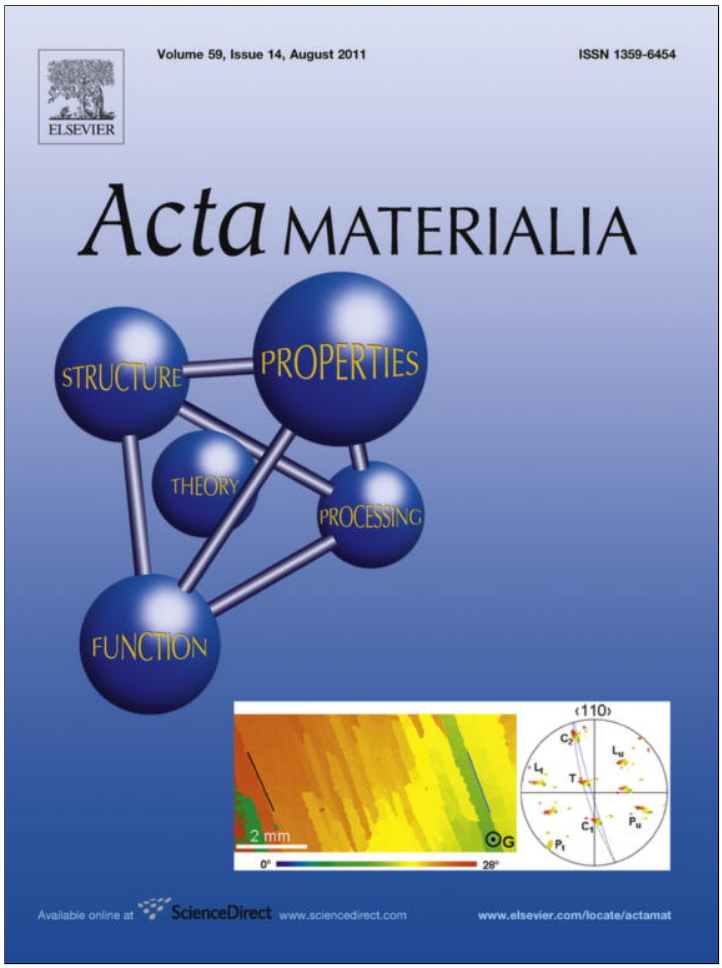

Available online at www.sciencedirect.com
ScienceDirect
Acta Materialia 59 (2011) 5603–5617
Acta MATERIALIA
www.elsevier.com/locate/actamat

Crystal plasticity of nanotwinned microstructures: A discrete twin approach for copper

Hamidreza Mirkhani, Shailendra P. Joshi *

Department of Mechanical Engineering, National University of Singapore, Singapore

Received 14 December 2010; received in revised form 18 May 2011; accepted 19 May 2011
Available online 16 June 2011

Abstract

This paper presents a discrete twin crystal plasticity (DT-CP) model for the size-dependent mechanics of nanotwinned (nt) metals. Specifically, it considers the length-scale-dependent yield response of nt-Cu [1] which exhibits a strengthening–softening transition of the yield strength below a critical twin thickness. The softening arising from source-governed preferential dislocation nucleation in the vicinity of the twin boundaries (TBs) competes with the strengthening arising from dislocation pile-up at TBs [2]. To incorporate the softening mechanism within the DT-CP model, a discrete twin-boundary-affected-zone (TBAZ) of thickness λ_z is introduced near each TB. This TBAZ is enriched by the kinetics of additional crystallographic slip arising from the profuse slip activity near a TB. The strengthening mechanism within a twin lamella is incorporated through internal stress on each slip system related to the average gradient of the excess dislocation density, introducing additional length-scale l_b which mimics the effectiveness of dislocation pile-up. With this framework, the orientation-dependent yield behavior of single grains with discrete twins is probed. These simulations qualitatively capture the experimental observations of the transition of the yield behavior from strengthening to softening as a function of λ. Some results for polycrystals with random orientations are also presented and compared with experiments. The DT-CP computational simulations provide useful insight into the microscopic activities in nt microstructures, which can be corroborated by experiments, and underscores the importance of discrete twin and TBAZ effects that should be accounted for in developing their corresponding homogenized descriptions.

Keywords: Nanoscale twins; Size-effects; Yield phenomena; Strengthening–softening transition; Crystal plasticity

1. Introduction

The Achilles heel of nanostructured metals has been the loss of ductility, despite being able to achieve significant strengthening over their conventional coarse-grained counterparts. Various strategies have been proposed to mitigate this problem (e.g. Ref. [3]). An attractive recourse is to engineer hierarchical micro-architectures that assist in strengthening by providing barriers to dislocation motion while concurrently retaining or introducing stabilizing mechanisms such as enhanced rate sensitivity and strain hardening. In the process of devising new micro-architectures, novel deformation mechanisms have been unraveled which may aid or adversely affect the objective [4–10]. Lu et al. [11] showed that, by introducing nanospaced TB within ultrafine-grained (ufg) copper (Cu), the yield strength can be increased substantially with decreasing TB spacing λ. This novel hierarchical microstructure, consisting of a nanotwinned (nt) architecture within a ufg polycrystalline mass, combines impressive strengthening, hardening and ductility [11,12] that is seldom observed simultaneously in nanocrystalline (nc) materials. More recently, Lu et al.'s uniaxial tension experiments on electrodeposited nt-Cu [1] over a larger range of TB spacing ($\lambda \sim 4$–100 nm), but with average grain size, $d \sim 500$ nm, similar to Ref. [11], shows intriguing response. As in previous work, this nt-Cu shows Hall–Petch-type strengthening for $15 \leqslant \lambda \leqslant 100$ nm. However, for $\lambda < 15$ nm, the yield strength decreases with decreasing λ to the extent that,

* Corresponding author. Tel.: +65 6516 4496, fax: +65 6779 1459.
E-mail address: Shailendra@nus.edu.sg (S.P. Joshi).

1359-6454/$36.00 © 2011 Acta Materialia Inc. Published by Elsevier Ltd. All rights reserved.
doi:10.1016/j.actamat.2011.05.036

for $\lambda \sim 4$ nm, it is nearly the same as that of its corresponding twin-free ufg counterpart with $d \sim 500$ nm. What is also interesting is the dramatically high hardening rate and, consequently, enhanced ductility in the 4 nm nt-Cu compared with the twin-free ufg-Cu attributed to novel mechanisms arising from TB–dislocation interactions [13].

Since the discovery of high-strength and ductile nt-Cu, several real and virtual experimental investigations have been performed to understand the mechanisms of twin-friendly materials, mainly Cu, including dislocation–twin interaction, twin evolution and stability of deformation [14–23]. At the continuum scale, the yield strengthening with decreasing twin thickness has been incorporated empirically via a Hall–Petch-type representation attributed to dislocation pile-up at TB within a crystal plasticity (CP) framework [12,24]. These models homogenize the discreteness of twins and incorporate their presence phenomenologically using plastically anisotropic slip laws along and across the TB. However, the intriguing transition from strengthening to precipitous softening [25] is a nascent observation which has not yet been incorporated within a CP framework. Although the strengthening–softening transition of yield strength has been reported and modeled in nc metals at small grain sizes ($d < \sim 15$ nm), the grain boundary (GB) mechanisms postulated there are probably not relevant in the nt microstructures in Ref. [1], given much larger grain size and the fact that the TBs are coherent, unlike the GBs. The quasi-three-dimensional (3d) molecular dynamics (MD) simulations [26] indicated that the effective critical resolved shear stress (CRSS) for dislocation nucleation in a single grain within polycrystalline nt-Cu decreased with decreasing λ. In other words, for a fixed grain size, slip activation became easier with increased TB density. Most recently, Li et al. [2] performed large-scale 3d-MD simulations on polycrystalline nt-Cu and proposed a novel softening mechanism to explain this transition, which is a function of both the grain size and TB spacing. It appeals to the preferential nucleation of dislocations [27,28] along TBs, which becomes profuse with decreasing λ owing to increasing TB–GB triple junctions (TJs), acting as potent dislocation sources. This enhances the dislocation-mediated plasticity in the vicinity of TB that manifests as defect generation within TB and TB migration.

This work presents a length-scale-mediated CP approach to capture the orientation-dependent mechanics of nt microstructures. Given the strong interest in nt-Cu, the formal development uses explicit information from the experimental and computational observations on nt-Cu. Unlike some of the previous CP models incorporating twinning in a phenomenological manner [12], the present work retains the discreteness of the twinned regions within a grain. Thus, an individual grain comprises discrete twin (DT) lamellas of equal thickness whose constitutive description includes enriched crystallographic slip laws to account for the strengthening and softening mechanisms observed in nt-Cu. This approach is referred to here as the discrete twin crystal plasticity (DT-CP). The strengthening of an individual grain is attributed to a length-scale-dependent internal resolved shear stress (IRSS) on each slip system due to a non-homogeneous distribution of excess dislocations between adjacent TBs, in addition to the RSS due to externally applied stimulus. The softening mechanism is incorporated as an additional slip activity on each slip system attributed to dislocations nucleated at the TJs [2] and pre-existing defects within the TBs [19,26]. To account for the softening contribution, a small but finite region designated a twin-boundary-affected-zone (TBAZ) is explicitly modeled in the vicinity of each TB within a grain. Thus, a single twin lamella is divided into two TBAZs that sandwich a parent region. The softening mechanism is a function of the TBAZ thickness λ_z and is active only in this region, while the strengthening mechanism is assumed to prevail in an average sense[1] over the entire twin lamella and is a function of λ. The next section briefly reviews the recent experimental and computational observations that provide the conceptual setting for this work. The subsequent sections derive the mechanics of DT-CP and use the governing expressions to solve numerical problems mimicking nt-Cu. First, the focus is on the response of a single grain under two-dimensional (2D) plane-strain conditions, and the yield strengthening–softening transition is investigated as a function of twin thickness and crystal orientation. Later, the approach is extended to polycrystalline simulations, and the trends are compared with the single grain results and experiments on nt-Cu.

2. Brief review of mechanisms in nt-Cu

The detailed transmission electron microscopy investigations [1,11,12] provide fundamental insight into some of the deformation processes that prevail in nt-Cu. Initially straight TB with no apparent dislocation debris in their vicinity show heavy dislocation pile-up, indicating that they act as strong barriers to dislocation motion. Along with the pile-up, some of the initially straight TB appear curved after deformation, indicating lattice incompatibilities. MD simulations [2,26] and experiments [20] indicate nucleation of Shockley partials ($1/6\langle 11\bar{2}\rangle$) at the TJs and across TBs [19], which manifest as steps on the TBs. Pre-existing defects within the TBs may also contribute to the overall plasticity with increasing TB density [2,19]. Dao et al. [12] postulated existence of a TBAZ at the TB whose thickness λ_z is $\sim$10 times the lattice parameter, irrespective of the TB spacing. This zone may be viewed as a region of profuse dislocation activity including preferred plastic slip along the twin plane (also a slip plane) and across it. In addition, at later stages of deformation, significant dislocation activity has been reported in the vicinity of the TBs, which may be a reason for the ductile response in nt-Cu. In précis, the key points from the experimental and MD

[1] As discussed later, this assumption is made only to partially ease the computational effort.

observations that form the basis of our DT-CP approach are:

1. Incipient dislocation activities in the vicinity of TB result in preferred slip modes along TB and pile-up across them.
2. The TJs act as special dislocation nucleation sources.
3. TB contain pre-existing defects that may trigger plasticity across them rendering them incoherent and may compromise their effectiveness as impenetrable barriers.
4. The TBAZ thickness on either side of a TB is, by definition, $\lambda_z = \min(\lambda, 2l_z)$, where $l_z = 5$ nm.

The present DT-CP approach focuses on the kinetics of crystallographic slip within the TBAZ to introduce the softening mechanism. Note that, for fixed λ_z, its significance increases as λ decreases.

3. Mechanics of length-scale-dependent strengthening–softening at yield: CP model

The DT-CP approach starts with decomposing the plastic slip on each slip system into two contributions: (a) slip due to pre-existing dislocations; and (b) additional slip arising from newly nucleated dislocations due to the presence of TB. Based on the observations summarized in the preceding section, two key length-scale-dependent mechanisms arising from the above-mentioned contributions are considered: (a) dislocation pile-up at the TB causing strengthening; and (b) preferred glide within TBAZ on slip planes aligned with the TB, contributing to the softening behavior.

The presence of dislocation pile-up at interfaces has been discussed within the context of discrete and continuum approaches [29–32]. As dislocations encounter TBs, they accumulate in a manner that can be measured in a continuum setting in terms of the geometrically necessary dislocation (GND) density ρ_g, which results in slip hardening. Similar to the rapid build-up of GND in the vicinity of GB at small grain sizes [33], it may be assumed that, in nt microstructures too, the GND density evolves rapidly, far exceeding the statistically stored dislocation (SSD) density controlling the flow stress at small strains. Further, within an individual grain of a heterogeneous microstructure such as in nt-Cu, ρ_g may vary between material points, setting up a GND density gradient $\nabla\rho_g$ which leads to a length-scale-dependent IRSS [34–36]. This additional non-local IRSS is adopted as the strengthening mechanism for each slip system, and it is accounted for in an average sense over the entire twin lamella thickness λ (Section 3.3).

To account for the softening, the TBAZ is modeled in the vicinity of a TB that hosts abundant sources of dislocation nucleation for both families of slip systems, namely along and across the TB. These sources along the TB are due to the TJ (i.e. TB–GB intersections) [2], while those across it are due to pre-existing defects within the TB [19,25,26]. As mentioned in Section 1, in the DT approach the TB and TBAZ are explicitly modeled. Naturally, the softening mechanism is present only within the TBAZ and depends on its thickness λ_z.

3.1. DT approach

Fig. 1a shows a schematic of the DT-CP approach defining key kinematic ingredients. An individual grain of average size d is divided by TB spaced equally at a distance λ. In this setting, the twinned and parent regions are indistinguishable and are referred to as the parent region in the discussion to discern them from the TBAZ. A TB is endowed with a TBAZ of fixed thickness λ_z on its either side (orange bands). Fig. 1b shows an individual twin lamella with a TBAZ and associated TB–GB TJ (red and purple lines[2]). In what follows, key kinematic and kinetic expressions are derived for the two regions, namely, the parent region and the TBAZ. Note that, within a typical twin lamella, the physical length-scales governing the strengthening and softening mechanisms may be different for different slip systems. Therefore, the 12 slip systems are categorized into two families: those that are along the TB (referred to as the α slip systems); and those that are across the TB (referred to as the β slip systems). Assuming that the dislocations newly nucleated from the special sources in the TBAZ are glissile, their contribution to the overall plasticity is accounted for as the additional plastic slip due to this mechanism, together with the slip arising from pre-existing dislocations (i.e. conventional slip). With this background, the slip rate on a slip system within a TBAZ (z) is written as

$$ {}_z\dot{\gamma}^i = \dot{\gamma}^i_s + \dot{\gamma}^i_{dz} \tag{1}$$

where $i = \alpha, \beta$ indicates the families of slip systems along and across a TB, respectively. The subscript s refers to the activities corresponding to the TJ and defects within TB, and dz refers to the conventional slip in the TBAZ.

In the parent region p, the special sources are not relevant, as the TB are sufficiently far away from it, and therefore ${}_p\dot{\gamma}^i = \dot{\gamma}^i_{dp}$.

3.2. Nucleation-induced plastic slip $\dot{\gamma}^i_s$ (TBAZ only)

The number of dislocation sources for the slip system along TB, N^α_s is [2]

$$N^\alpha_s = p^\alpha \frac{d}{b} \tag{2}$$

where b is the magnitude of the Burgers vector, and p^α is a fraction constant close to unity, indicating the effectiveness of the emission sites (Fig. 2a). Similarly, on the β slip systems that may also host nucleation sources in the form of pre-existing defects within a TB, the corresponding number of dislocation sources $N^\beta_s = p^\beta d/n_a b$, where $n_a b$ represents the average spacing between consecutive steps at the TB

[2] For interpretation of color in Figs. 1–11, the reader is referred to the web version of this article.

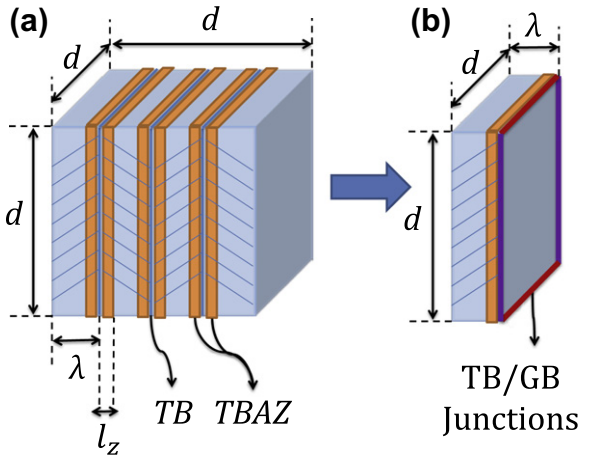

Fig. 1. (a) Schematic of the DT model. A single cubic grain comprises twin lamellae of equal thickness. The orange bands adjacent to TB are TBAZs. (b) Enlarged view of of single lamella. The red and purple lines constitute TB–GB TJ.

(Fig. 2b). For simplicity, it is assumed that $n_a = 1$, giving $N_s^\beta = p^\beta a/b$. If a single dislocation travels distance x_i^α along a TB over distance d, its contribution to the total displacement is $bx_i^\alpha/d (0 \leqslant x_i^\alpha \leqslant d)$. In this work, it is assumed that, when this special mechanism governs initial plasticity within the TBAZ, the nucleated dislocations responsible for it do not experience substantial obstacles as they traverse parallel to the TB [20].[3] As such, at least during the incipient plasticity governed by this mechanism, one may assume $x_i^\alpha = d$, resulting in the total displacement in TBAZ along the TB direction, ${}_zD^\alpha = N_s^\alpha b$ (Fig. 2). The corresponding plastic slip γ_s^α on the α family due to this mechanism is

$$\gamma_s^\alpha = \frac{{}_zD^\alpha}{\lambda_z} = \frac{N_s^\alpha b}{\lambda_z} \approx p^\alpha \frac{d}{\lambda_z} \tag{3}$$

Note that this plastic slip contribution depends on the TBAZ thickness λ_z.[4] Similarly, for the across-slip systems, the plastic slip contribution γ_s^β (i.e. due to pre-existing defects within TB) is $\gamma_s^\beta = N_s^\beta b/t_2$, where, as shown in Fig. 2b, $t_2 = q\lambda_z/\cos\phi^i \approx cq\lambda_z$, the constant q is a geometrical factor to accounts for the imperfection of the swept area covered by some plastic slips, and ϕ^i is the angle between ith slip system and the TB. From Eqs. (2) and (3), the plastic slip on the ith slip system family can be written as

$$\gamma_s^i = p^i \frac{d}{cq\lambda_z} \qquad (i = \alpha, \beta) \tag{4}$$

where $c = 1 (\phi^i = 0)$ for the family of $i = \alpha$ and $c \approx 1.73$ ($\phi^i = 54.7°$) for $i = \beta$; for $\lambda \ll d$, $q \approx 1$. In arriving at Eq. (4), it is implicitly assumed that all possible sources of nucleation are activated. Accounting for the activation probability of dislocations through Debye frequency, the plastic slip rate on each slip system is [2]

$$\dot\gamma_s^i = P_{act} p^i \frac{d}{c\lambda_z} = p^i \frac{d}{cq\lambda_z} v_D \exp\left(-\frac{\Delta U_{nuc}}{k_B T}\right) \exp\left(\frac{S\tau_0^i V^*}{k_B T}\right) \qquad (i = \alpha, \beta) \tag{5}$$

where P_{act} is the probability function related to the Debye frequency v_D, activation energy for dislocation nucleation ΔU_{nuc} [27], effective RSS τ_0^i, activation volume V^*, Boltzmann constant k_B and temperature T, and S is a factor that distributes the local stress amplification over the TBAZ. On an ith slip system within the α and β families, τ_0^i is defined as $\tau_0^i = \tau_{ext}^i - \tau_b^i$, where τ_{ext}^i is the RSS due to externally applied loads, and τ_b^i is the length-scale-dependent IRSS generated due to the non-homogeneous dislocation pile-up along the ith slip system within a twin lamella. For a characteristic slip rate $\dot\gamma_s = \dot\gamma_0$ at which external stimulus initiates plastic slip, one may identify τ_{ext}^i as the CRSS τ_c^i for the source-governed plastic slip. Inverting Eq. (5) and rearranging, one obtains[5]

$$\underbrace{\tau_c^i}_{\text{Total slip resistance}} = \tau_0^i + \tau_b^i = \left(\underbrace{\frac{\Delta U}{SV^*}}_{\text{Athermal slip resistance}} - \underbrace{\frac{k_B T}{SV^*} \ln\left[\frac{p^i}{c}\left(\frac{d}{\lambda_z}\right)\frac{v_D}{\dot\gamma_0}\right]}_{\text{TBAZ induced thermal softening}} \right) + \underbrace{\tau_b^i}_{\text{IRSS}} \tag{6}$$

From a computational viewpoint, it is attractive to use a power-law form of the crystallographic slip [38]. Therefore, within TBAZ the evolution of plastic slip on each slip system is assumed to be

$${}_z\gamma_s^i = \dot\gamma_0 \left(\frac{\tau_{ext}^i}{\tau_0^i + \tau_b^i}\right)^{1/m_z} sgn(\tau_{ext}^i) \tag{7}$$

where m_z is the rate-sensitivity index of the TBAZ.

We note in passing that dislocation nucleation at the TJs may cause migration of TBs under applied shear stress [10,20,39]. Such processes cause growth of some twin lamellas at the expense of others within a given crystal, modulating the strengthening mechanisms.

[3] As the deformation progresses, slip hardening occurs within the TBAZ due to novel hardening mechanisms [37]. These are accounted for in a phenomenological way through the latent hardening parameters in the slip hardening functions (Section 3.2).

[4] If instead, one chose to homogenize the source-induced plasticity over the twin lamella, Eq. (3) would be written for the entire lamella in an average sense by substituting λ instead of λ_z.

[5] The grain size d appears in Eq. (6) because it is assumed to be constant on an average. A more rigorous implementation should account for the variations in the grain size in three dimensions due to arbitrary grain shape. This would require that the actual length of an individual TB at a given position in a given direction should replace d in describing τ_0^i for each slip system.

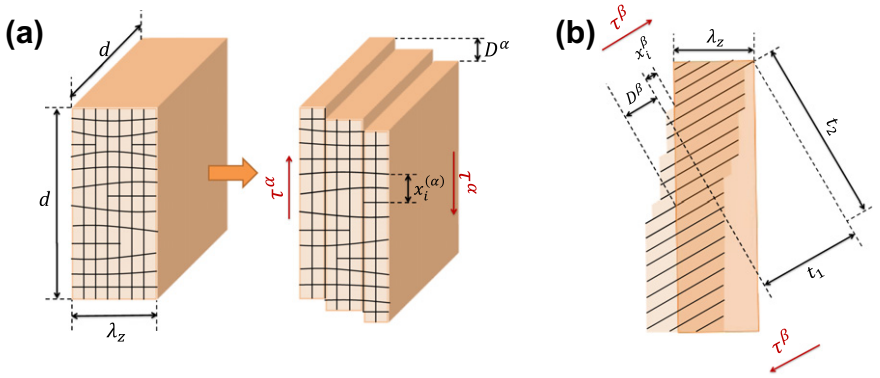

Fig. 2. Plastic slip within TBAZ (a) along α slip system due to TB–GB TJ, and (b) along β slip system due to TB defects.

3.3. TB-induced strengthening (parent and TBAZ)

As mentioned earlier, the TB-induced strengthening is attributed to the IRSS τ_b^i (Eq. (6)) that develop owing to non-homogeneous pile-up of the GND density at interfaces. This strengthening captures the Hall–Petch-type behavior [34] in microstructures with plastically hard interfaces and is given as [34,35]

$$\tau_b^i = Dl_b^2 \nabla \rho_g^i = Dl_b^2 \nabla^2 \gamma^i \qquad (i = \alpha, \beta) \tag{8}$$

where ∇ indicates the gradient along the slip direction, and D is the effective elastic stiffness related to the shear modulus and Poisson's ratio [34]. A notable feature of Eq. (8) is that the IRSS-induced strengthening may be different on different slip systems. This is indeed the case in the nt-Cu [1], where the GB are spaced much further apart compared with the TB; consequently, the strengthening of the α slip systems is expected to be much smaller than that of the β slip systems. The IRSS-induced strengthening may prevail over a significant portion of the twin lamella thickness and not just TBAZ. This may be reflected by setting the internal length-scale l_b, which indicates the extent over which the effect of IRSS will be felt over a twin lamella to be greater than the TBAZ thickness.

Although Eq. (8) has several attractive features, its rigorous implementation within a finite-element (FE) framework requires calculation of first gradients of the GND density (i.e. second gradients of plastic slip) on each slip system, which is computationally expensive. This computational expense is in addition to the cost incurred by the fact that the present approach considers discrete twins and their TBAZs. Therefore, to ease some of the effort, an approximation of Eq. (8) is adopted here, but the main idea is retained. To first order, the GND density gradient $\nabla\rho_g$ in Eq. (8) may be approximated as an average quantity $\sim \bar{\rho}_g/\lambda$, where $\bar{\rho}_g\left(=\frac{1}{V_t}\int_{V_t}\rho_g dV_t\right)$ is the average GND density over an individual twin lamella volume V_t. Then, Eq. (8) may be simplified as

$$\bar{\tau}_b^i \approx Dl_b^2 \frac{\bar{\rho}_g b \sin\phi^i}{\lambda} \tag{9}$$

Eq. (9) significantly eases the computational expense, because the IRSS can now be accounted for as an anisotropic material parameter for each slip system. However, two important differences exist between Eqs. (8) and (9). First, Eq. (8) indicates that, for a fixed λ, the IRSS varies along the slip direction with a high value at the TB which smoothly decays away from it. However, Eq. (9) essentially results in a constant (homogenized) IRSS on the ith slip system in a typical twin lamella. Secondly, recent calculations show that the IRSS (Eq. (8)) tends to saturate below a certain lamella thickness, λ_{cut} [34]. From a mechanistic viewpoint, this happens because it becomes difficult to induce increasingly higher lattice curvatures, owing to strong resistance from the GND density to the plastic slip. Mathematically, the governing partial differential equation becomes increasingly stiff. Mechanism-based arguments from experiments and MD simulations [12,37] also indicate that, below a certain microstructural size on the order of 10–15 nm, the pile-up does not evolve or becomes difficult. This second aspect is lost in the homogenization and gives ever-increasing internal stress with decreasing thickness. To mimic the mechanics of pile-up, a cut-off thickness $\lambda_{cut} = 15$ nm is introduced, below which $\bar{\tau}_b^i$ is assumed to be independent of the twin thickness. Note here that a constant internal stress below λ_{cut} is an idealization. A more realistic scenario would be to assume a decreasing internal stress with decreasing λ below this critical thickness as dislocation pile-up becomes increasingly difficult [13,37].[6] However, it is demonstrated later that, even with this conservative assumption, the softening mechanism dominates the overall response, resulting in the drop in the yield strength below λ_{cut}. Finally, in the approximation (Eq. (9)), the latent hardening effect owing to the GND density variation on other slip systems is not explicitly modeled, but may be accounted for through the latent hardening coefficients [38].

[6] The precise nature of the internal strengthening will depend on the active mechanism. If one assumed that the internal stresses exist only because of the pile-up mechanism, the lack of it would result in the lack of internal stresses. However, this is probably an extreme case, as a different, albeit weaker, mechanism may exist below a critical thickness [13].

3.4. Final expressions for slip rates

Sections 3.1–3.3 focused on developing constitutive equations for the contribution from the nucleation-induced slip rate to the total slip rate within the TBAZ. However, the total slip rate within TBAZ must also include the contribution from pre-existing dislocation density (Eq. (1)). The same power-law form [38] is adopted for this contribution. Thus, the total plastic slip rate in a TBAZ is

$$ {}_z\dot{\gamma}^i = \left[\underbrace{\dot{\gamma}_0 \left(\frac{\tau^i_{ext}}{\tau^i_0 + \bar{\tau}^i_b} \right)^{1/m_z}}_{\dot{\gamma}_s} + \underbrace{\dot{\gamma}_0 \left(\frac{\tau^i_{ext}}{g^i} \right)^{1/m_z}}_{\dot{\gamma}_{dz}} \right] sgn(\tau^i_{ext}) \tag{10a} $$

Similarly, the plastic slip rate in the parent region is also assumed to follow power law and is given by

$$ {}_p\dot{\gamma}^i = \left[\underbrace{\dot{\gamma}_0 \left(\frac{\tau^i_{ext}}{g^i} \right)^{1/m_p}}_{\dot{\gamma}_{dp}} \right] sgn(\tau^i_{ext}) \tag{10b} $$

where m_p is the rate sensitivity index for the parent region, and

$$ \begin{aligned} g^i &= g^i_0 + \bar{\tau}^i_b + \int_0^t \dot{g}^i dt \\ \dot{g}^i &= \sum_{k=1}^{n} h_{ikj} \dot{\gamma}^{(k)} (j = z, p) \\ h_{ii} &= h_0 \sec h^2 \left| \frac{h_0 \dot{\gamma}}{\tau_s - \tau_0} \right| \quad \text{(no sum on } i\text{)} \\ h_{ik} &= \eta h_{ii} \end{aligned} \tag{11} $$

Eqs. (10a) and (10b) include the possibility of the rate sensitivity indices being different for the parent region (m_p) and TBAZ (m_z) [12]. In Eqs. (11), g^i_0 is the initial (length-scale-independent) slip resistance that is also augmented by the IRSS contribution, and h_{ik} is the matrix of self and latent hardening coefficients which evolves according to Eq. (11c and d) with total plastic slip $\bar{\gamma}$, initial hardening modulus h_0, saturation stress τ_s and the latent hardening coefficient η [38]; t is the current time, and n is the total number of slip systems. Zhu et al. demonstrated that loss of TB coherency with deformation [37] is a special hardening mechanism in the proximity of TB. Although it is assumed that τ^i_0 does not evolve with deformation for the TBAZ, its corresponding plastic slip ${}_z\dot{\gamma}^i_s$ is accounted for in the evolution of slip systems' hardening (Eq. (11b)). The enhanced hardening within the TBAZ is phenomenologically accounted for, at least partially, through (a) the dependence of the self-hardening on the accumulated slip on a given slip system, which includes both the contributions (Eq. (11b)) and (b) ascribing a high latent hardening coefficient $\eta = 2$.

4. Material parameters

The elastic properties for Cu are $C_{11} = 168{,}400$ MPa, $C_{12} = 121{,}400$ MPa, and $C_{44} = 75{,}400$ MPa [24]. The length-scale-independent slip system properties are assumed to be similar to those of bulk single crystal pure Cu: $g_0 = 60$ MPa, $h_0 = 541$ MPa and $\tau_s = 109$ MPa [38,40].

4.1. Average IRSS $\bar{\tau}^i_b$

In nt microstructures with the grain size much larger than the TB spacing [25], the IRSS $\bar{\tau}^\alpha_b$ on the α slip systems (i.e. along the TB) is expected to be much smaller than those across them. Therefore, as a limiting case, we assume $\bar{\tau}^\alpha_b = 0$. Therefore, it is the internal stress on the β slip systems that is of interest. Table 1 lists the calculated values for $\bar{\tau}^\beta_b$ (Eq. (9)), and the parameters involved in obtaining the values are briefly discussed.

To calculate $\bar{\tau}^\beta_b$, estimates of l_b and $\bar{\rho}_g$ are required. The interpretation and choice of l_b is an open issue within the enriched continuum mechanics frameworks, but a general consensus is that it is expected to be problem-dependent and, for a given problem, it may evolve with deformation [41]. Arguments based on statistical mechanics [36] suggest a length-scale related to the dislocation spacing ($\sim 1/\sqrt{\rho}$), whereas those based on thermodynamic coarsening [41] indicate it to be on the order of average slip plane spacing ($\sim 100b$, b = magnitude of Burgers vector). For most problems in the nc regime, these give an estimate of l_b which ranges between tens [41] and hundreds [36] of nanometers. Another interpretation of l_b is to ask: What is the minimum microstructural size above which the dislocation pile-up mechanism can be effective? For nc materials, this lower-bound estimate is also in the range ~10–15 nm, below which dislocation pile-up is difficult [12,37]. Thus, there is a range that one could choose from, and a constant value of $l_b = 15$ nm is assumed here for all the cases. Incidentally, the last of the aforementioned interpretations may also provide a basis for the cut-off twin thickness below which the internal stress ceases to evolve with decreasing λ in a manner given by Eq. (9).

To estimate $\bar{\rho}_g$, we refer to two insightful observations. Lu et al. [1] report a high dislocation density ranging between $\sim 10^{14}\ \mathrm{m}^{-2} (\lambda = 96\ \mathrm{nm})$ and $\sim 5 \times 10^{16}\ \mathrm{m}^{-2} (\lambda = 4\ \mathrm{nm})$. Although not all the dislocations will be GNDs,

Table 1
Parameters used for calculation of the CRSS for nucleation-induced slip, τ^i_0 (Eq. (6)).

ΔU_{nuc} (eV)	k_B ($\mathrm{m^2\ kg\ s^{-2}\ K^{-1}}$)	T (K)	V^* ($\mathrm{m^3}$)	d (m)	r_v
1.0	$1.3806503 \times 10^{-23}$	287	7.92×10^{-29}	500×10^{-9}	3.11×10^{14}

Table 2
Calculated τ_0 (Eq. (6)) and $\bar{\tau}_b$ (Eq. (9)) on both families of slip systems.

λ (nm)	100	40	15	10	8	4
$\tau_0^{\alpha}, \tau_0^{\beta}$ (MPa)	82, 115	82, 115	82, 115	82, 115	74, 108	51, 85
$\bar{\tau}_b^{\alpha}, \bar{\tau}_b^{\beta}$ (MPa)	0, 55	0, 136	0, 364	0, 364	0, 364	0, 364

we assume that a sizable proportion, especially on the β slip systems, may appear so, because they are blocked by the TB. This provides a rough range for $\bar{\rho}_g$. The second observation comes from Zhu et al. [37] who indicate that the limiting shear stress above which a dislocation may pass through a TB is in the range ~300–400 MPa for $\lambda \sim 15$–10 nm. In the present calculations, this range may be viewed as the limiting IRSS (on β slip systems) that can be offered by the TB for $\lambda = 15$ nm. These two observations, together with $l_b = 15$ nm, provide an estimate of $\bar{\rho}_g \sim 8 \times 10^{14}\ \mathrm{m}^{-2}$, which is kept constant for simplicity. This estimate of $\bar{\rho}_g$ will vary somewhat, depending on the choice of l_b.

4.2. CRSS for the nucleation-induced slip in TBAZ, τ_0^i

Comparing Eq. (6) with the one derived in Ref. [2], one obtains the direction-dependent CRSS τ_0^i, which determines the contribution of the additional plasticity due to TB-induced dislocation nucleation for the slip systems within the TBAZ. In the process, the parameter in Eq. (6) which is calibrated with the experiments [1] is the ratio $r_v = pv_D/\dot{\gamma}_0$. The r_v's are calculated for λ =15, 10, 8, and 4 nm by comparing their macroscopic shear yield stresses with Eq. (6) and an average value is adopted. Table 2 lists the values [2] for the parameters in Eq. (6). Note that with $\lambda_z = 5$ nm, the entire twin assumes the role of the TBAZ, so that $\lambda_z = \lambda$ below 10 nm. Table 2 gives the numerical values for τ_0^i calculated from Eq. (6).

4.3. Rate sensitivity index

From the viewpoint of activation volume, the profuse dislocation activity within TBAZ renders it more rate sensitive compared with the parent region [37]. Therefore, $m_z = 0.067$ is chosen for the TBAZ and $m_p = 0.01$ for the parent region [12] in Eqs. (10a) and (10b). Note that, unlike homogenized approaches [12,24], where the effective rate sensitivity is used as a volume-averaged function of λ, in the present work such averaging is not necessary, as the twin lamellas and TBAZ are explicitly modeled.

5. Computational models and numerical results

The constitutive description elaborated in the preceding sections is implemented as a crystal plasticity user-material subroutine (CP-UMAT) within ABAQUS/STANDARD [38]. Supplementary material briefly discusses the numerical implementation of the constitutive laws outlined in the preceding section [42]. Although polycrystalline models would be the best choice to compare the response of nt-Cu simulations with experiments, there are benefits in investigating the single grain responses. Foremost, the DT approach is computationally much more expensive in a polycrystalline setting compared with single grain simulations (Supplementary material). Secondly, the trends in single grain simulations can be investigated in detail as a function of crystal orientation and TB spacing. Therefore, the following section first describes the results for single grain models. Later, the results for polycrystalline nt-Cu are briefly presented.

5.1. Single grain models

Consider a plane-strain single grain setting subjected to uniaxial loading along the X direction. This enables investigation of the effect of TB spacing λ as a function of crystal orientation. Fig. 3a shows the plane within a face-centered cubic (fcc) structure that is considered here, which is the plane comprising $\langle 1\,1\,0\rangle$ (*global X*) and $\langle 0\,0\,1\rangle$ (*global Y*) directions. The (1 1 1) twin plane (i.e. TB) intersects the X–Y plane and makes an angle θ with the loading direction, which may also be referred to as the crystal orientation. Fig. 3b shows a typical computational model with $\theta = 54.7°$, comprising multiple twin lamellas and their TBAZ. The number of twin lamellas depend on θ and λ; four orientations, $\theta = 54.7°$, 24.7°, 9.7° and 0°, and five TB spacings, $\lambda = 100$, 40, 15, 10, 8, and 4 nm, are considered for each orientation. As indicated in Fig. 3b, the kinematic boundary conditions (bc) are applied such that the top and bottom edges are free to move vertically, but constrained to remain straight. The left edge is also constrained from moving in the X direction, and a constant velocity bc is applied at the right edge such that the nominal applied strain rate $\dot{\bar{\varepsilon}} = 1 \times 10^{-3}\ \mathrm{s}^{-1}$. For convenience, d (i.e. computational cell) is set equal to 500 nm × 500 nm.

5.2. Overall behavior

Fig. 4a and b shows the macroscopic tensile response of a single nt grain with $\theta = 54.7°$ as a function of λ for the strengthening–softening and strengthening-only cases, respectively. The former refers to the slip laws that include the softening term and TBAZ, whereas in the latter the TBAZ is not modeled and therefore, the softening mechanism is not accounted for. Owing to the lack of back stress on the along slip systems, the overall behavior is expected to be controlled by their Schmid factor measured with respect to the loading axis. Therefore, single grain model with $\theta = 54.7°$ is expected to be the softest orientation amongst all the θ's considered in this work. For consistent comparison across different orientations, yield strength σ_y is defined as the stress corresponding to 0.5% proof strain. The plots also include the response of a twin-free single crystal.

As indicated in Fig. 4a, the stress–strain response exhibits a strengthening trend up to $\lambda = 15$ nm (λ_{cr}), but the yield

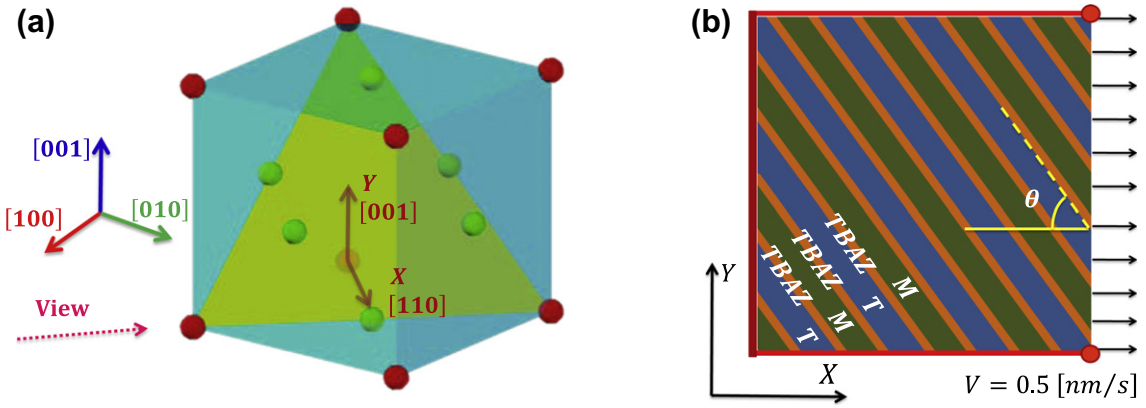

Fig. 3. (a) Schematic of an fcc crystal showing the X–Y plane considered in the plane strain FE model in (b). In (a), the twin plane (triangle) intersects the X–Y plane that forms angle θ with the loading (X) direction. In (b) a quasi-static velocity V is applied at the right edge; the top and bottom edges are constrained to move along with the top and bottom control points, respectively (red circles). The left edge is also constrained to move only along the Y direction.

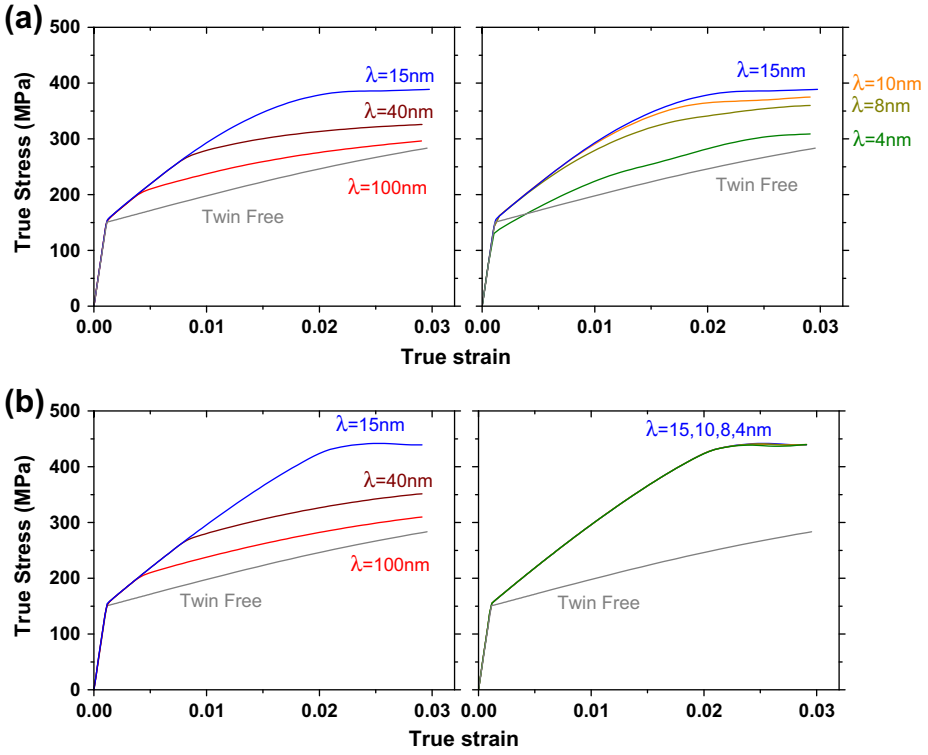

Fig. 4. True stress–true strain response of single grain nt-Cu with $\theta = 54.7°$as a function of TB spacing from (a) strengthening and softening model, and (b) strengthening-only model.

strength decreases with further decrease in the TB spacing. Unlike Fig. 4a, the strengthening-only response in Fig. 4b shows saturation for $\lambda \leqslant 15$ nm, because of the saturation of the IRSS below λ_{cr}. These results are discussed further within the context of strengthening and softening contributions (Eq. (10)).

Fig. 5 shows the macroscopic yield strength σ_y (i.e. at $\bar{\varepsilon} = 0.5\%$) as a function of λ for different θ's. These strengthening–softening trends are qualitatively comparable with the experiments [1] and MD simulations [2,26]. Notably, even for $\theta = 0°$ that has a zero Schmid factor for the softer α slip systems, a small but finite drop in σ_y is observed below λ_{cr}. This is because of the activation of the β slip systems, contributing to the overall softening in the case of $\theta = 0°$. Accounting for the effect of the softening mechanism, in all orientations, not only does the macroscopic flow stress drops below λ_{cr}, but for all λ's the yield strengths are also lower compared with their strengthening-only counterparts (e.g. Fig. 4a and b). This indicates that the softening mechanism is present even when

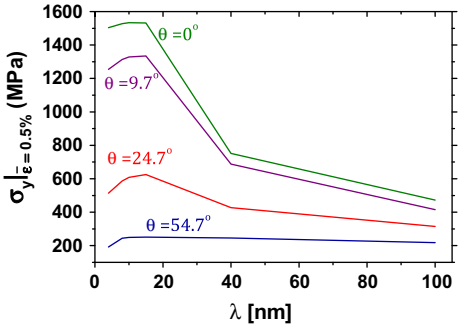

Fig. 5. Twin thickness (λ) dependent macroscopic yield strength (σ_y) of single grains with different orientations (θ).

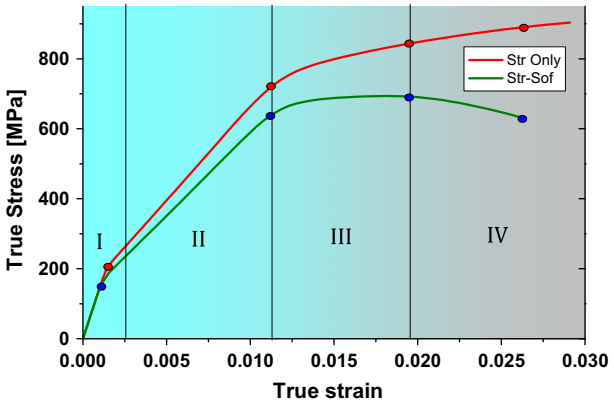

Fig. 6. True stress–true strain response for $\lambda = 4$ nm, $\theta = 24.7°$, for the strengthening-only case, and in the presence of softening.

$\lambda > \lambda_{cr}$, although it does not dominate the IRSS-induced strengthening. Its effect on the overall response is strongly felt below λ_{cr}.

In Fig. 4, the stress–strain curves for all the orientation, except for $\theta = 0°$ share some common characteristics. First, an initial yield exists where a stress–strain curve departs from linearity. This departure is attributed to the slip governed by g_0 on the α slip systems in the parent region and TBAZ owing to lack of IRSS on those slip systems. The stress at which it occurs is independent of λ for $\lambda > 4$ nm. This is because, for $\lambda > 4$ nm, $g_0 < \tau_0$ for the α slip systems, and it is only for $\lambda > 4$ nm that $\tau_0 < g_0$ (Table 2). This aspect is discussed further in the next paragraph. Secondly, the initial yield is followed by a region of strong hardening that evolves at a constant rate until the β slip systems are activated, which is marked by a dramatic change in the slope of the stress–strain responses. This macroscopic yield signifies profuse overall slip activity. The macroscopic yielding depends strongly on λ, which indicates increasing strength with decreasing λ up to 15 nm and a reversal in the trend below λ_{cr}.

It is of interest to probe further the behavior of a microstructure where the softening contribution is dominant. Therefore, we discuss the case with $\lambda = 4$ nm and $\theta = 24.7°$ as it exhibits several interesting characteristics highlighting the contributions from the softening mechanism (Fig. 6). On the basis of the hardening evolution (see also Supplementary material), the stress–strain responses in Fig. 6 may be divided into four regions:

1. Regions I and II, which includes the incipient yield and an overall hardening response with a constant hardening rate: as mentioned earlier, for this specific case the initial yield occurs earlier in the presence of the softening mechanism compared with its strengthening-only counterpart, because $\tau_0 (= 51$ MPa$) < g_o (= 60$ MPa). Thus, this regime is governed by the nucleation-driven slip activity on the α slip systems in the TBAZ. Similarly, the hardening rate is also smaller in the former compared with the latter. An interesting question arises as to why the macroscopic response in this regime exhibits hardening while the underlying plasticity is non-hardening (see Eq. (10a) and its discussion). For the sake of brevity, the details pertaining to this macroscopic hardening response at small twin thicknesses are omitted here, but are included in the Supplementary material.
2. Regime III in which other slip systems are activated and is signified by a reduction in the initial hardening rate: this reduction is larger in the presence of the softening term because it also weakens of the β slip systems compared with the strengthening-only case.
3. Regime IV, is where the overall response for the strengthening–softening model shows a decrease in the stress: this is probably a result of concentrated preferential slip along TB (not shown for brevity). Whether such a unidirectional slip within a twin manifests itself as TB migration [18] is beyond the scope of this work.

5.3. Micro-mechanical behavior

One of the advantages of the DT-CP model is that it allows resolving the heterogeneity of the local slip within individual lamella and associated TBAZ. To illustrate the similarities and differences in the distribution of the total plastic slip ($\bar{\gamma}$) as a function of λ, diagonal paths are defined between the bottom-left and top-right corners of the single grain models with $\theta = 54.7°$. Fig. 7a–c shows the evolution of $\bar{\gamma}$ along the normalized diagonal distance for different λ's. For comparison, Fig. 7d shows the distribution of $\bar{\gamma}$ for the strengthening-only case ($\theta = 54.7°$, $\lambda = 100$ nm). For $\lambda = 100$ nm (Fig. 7a), $\bar{\gamma}$ is initially (at $\bar{\varepsilon} = 0.5\%$) nearly homogeneous, but gets localized within the TBAZ with increasing applied strain. At this stage, the total slip is dominated by the activity on the α slip systems. In comparison, for the strengthening-only case (Fig. 7d) the TBAZ is not modeled, and the relative slip activities in the lamellas are determined mainly by their Schmid factors.

It is interesting to note that the plastic slip distributions for $\lambda \leqslant 15$ nm (Fig. 7b and c) indicates zones of large plasticity closer the bounding edges of the grains. As shown in Fig. 8a–d, this gives rise to a central core within a grain

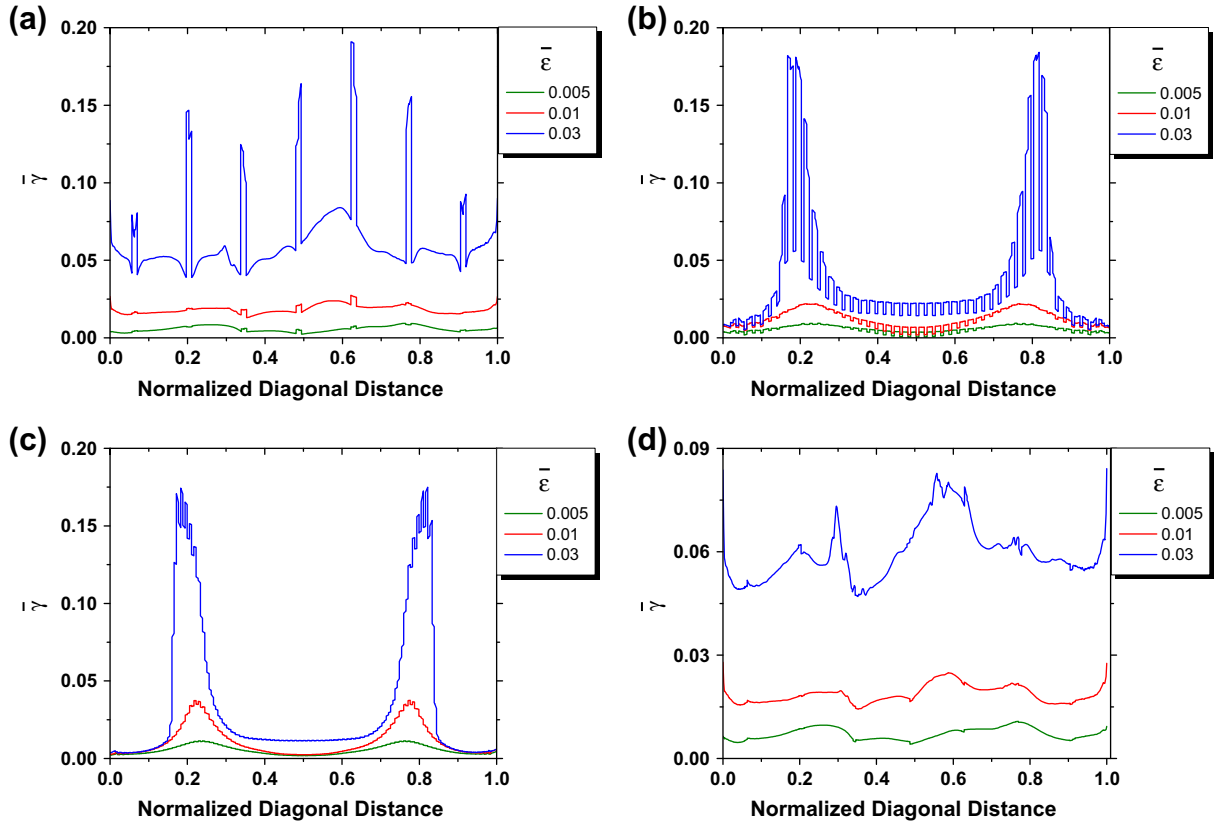

Fig. 7. Evolution of total plastic slip along normalized diagonal for the strengthening–softening single grain model ($\theta = 54.7°$) with (a) $\lambda = 100$ nm, (b) $\lambda = 15$ nm, and (c) $\lambda = 4$ nm; (d) shows the plastic slip evolution for the strengthening-only case with $\lambda = 100$ nm.

that experiences a relatively lower slip compared with the regions closer to the grain edges. The spatial distribution of plastic slip within the grain suggests that it experiences a torque as a result of resistance, offered by the hard bc imposed on the grain edges (Section 5.1), to the free lattice rotation caused by preferential shearing along TB, roughly mimicking single slip. An enlarged view (Fig. 8d) clearly shows that the TB experience a curvature (indicated by yellow traces) due to the induced torque. This observation of curved TB is consistent with experiments [12] and MD simulations [23], suggesting that TB curvature arises from the constraint imposed at the GB against tensile axis rotation under single slip-like conditions that are accentuated by high TB density at very small twin thicknesses. The other orientations considered in the present work also exhibit similar behavior (e.g. Fig. S2a–d, Supplementary material), but its effect is the most discernable for $\theta = 54.7°$, given its high Schmid factor. As discussed in Section 6.2, this phenomenon is also observed in grains within a polycrystalline setting, albeit to a lesser degree, as the constraint offered by neighbouring grains may not be as strong as the one assumed here in the single grain models.

6. Polycrystal simulations

The results of polycrystal simulations comprising grains with discrete twins and TBAZ are now presented. As in the preceding section, the individual grains are 500×500 nm. Two sets of polycrystals are chosen: (a) a 6×6 matrix consisting of single grains with the same four grain orientations investigated in the preceding section (Section 5), but arranged randomly within the polycrystal (Fig. 9a); and (b) a 6×6 polycrystal with random grain orientations (Fig. 9b). Case (a), wherein the volume fraction f_0 of each grain orientation is 25%, is chosen to compare the polycrystal characteristics with their single grain counterparts. For both cases, symmetric bc are applied at the left and bottom edge of polycrystals, and a uniform velocity $v = 3$ nm/s is applied at the right edge to give a nominal strain rate of $\dot{\bar{\varepsilon}} = 1 \times 10^{-3}$ s^{-1}. For each case, the simulations are performed for $\lambda = 100$, 40, 15, 10, 8 and 4 nm.

6.1. Macroscopic behavior

Fig. 10 summarizes the variation of σ_y as a function of λ for both the cases together with the experimental results of Lu et al. [1]. As grain size effect is not accounted for in the present work,[7] the experimental values are plotted after deducting its contribution (corresponding to the ufg-Cu [1,43]) from the overall strength. For comparison, the

[7] The grain-size effect has been removed from the experimental result ($15 \leqslant \lambda \leqslant 96$ nm) by deducting the Hall–Petch contribution $\Delta\sigma_y = kd^{-0.5}$, with $k = 3266$ MPa $\sqrt{\text{nm}}$ and d = 500 nm [2].

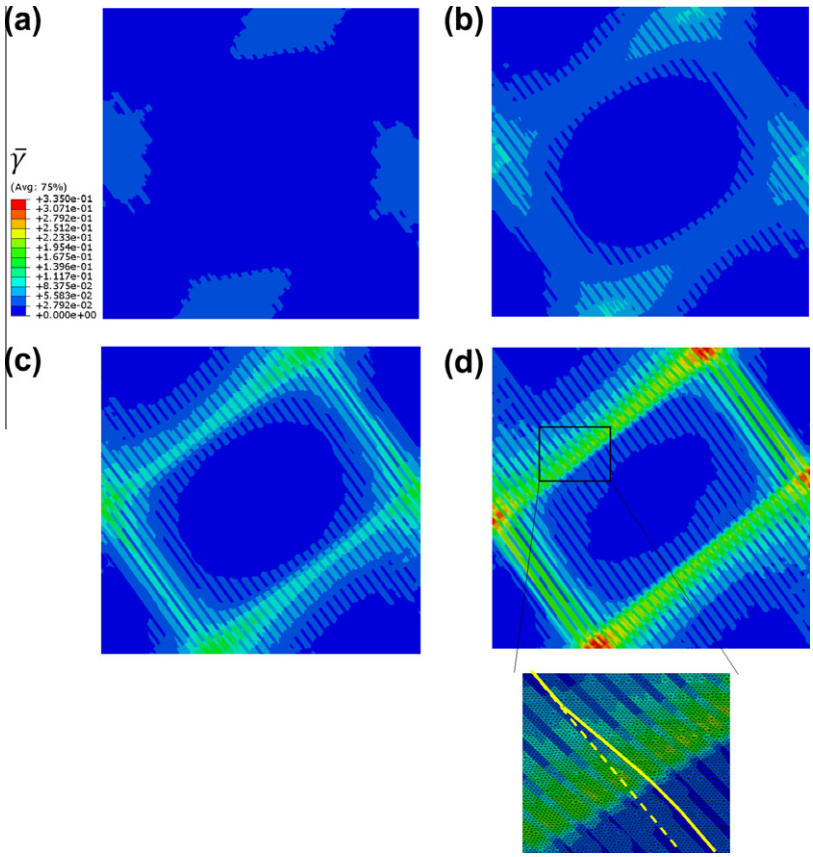

Fig. 8. The contour plot of cumulative plastic slip $\bar{\gamma}$ for the single grain with $\theta = 54.7°$ and $\lambda = 15$ nm at (a) $\bar{\varepsilon} = 0.01$, (b) $\bar{\varepsilon} = 0.015$, (c) $\bar{\varepsilon} = 0.02$, and (d) $\bar{\varepsilon} = 0.03$. As deformation progresses, shear slip starts to localize at the boundary zones with more stress concentrations. The enlarged view in (d) shows the trace of a curved TB (yellow solid line) compared with its original undeformed position (yellow dashed line).

figure includes simple homogenized estimates based on the single grain results (Section 5) using the Taylor (rule-of-mixture—ROM) and Sachs (inverse rule-of-mixture—iROM) models which assume equal f_0. Several salient features can be extracted from Fig. 10. The Taylor homogenization of single grain models predicts highest strengthening at the transition size, dominated by the strongest grain orientation ($\theta = 0°$), while the Sachs homogenization predicts the lowest strengthening dictated by the softest orientation ($\theta = 54.7°$). It is known that these simple estimates better represent polycrystalline behavior that sample sufficient number of grains with sufficient number of grain orientations [44,45]. Therefore, the present homogenized results derived from the limited single grain models should only be viewed as useful in providing rough bounds rather than an accurate quantitative estimate. In the Sachs model, individual grains within a polycrystal are assumed to experience the same state of stress, whereas the Taylor model assumes iso-strain conditions. These are highly idealized assumptions and, in real materials as well as in FE simulations, the conditions are intermediate between these extremes. Against this backdrop, it is interesting to note that the Taylor assumption shows a reasonable corroboration with experiments for $\lambda > 15$ nm, whereas the Sachs assumption tends to capture the softening regime better. One hypothesis could be that the real polycrystalline nt microstructures in the strengthening regime ($\lambda > 15$ nm) may resemble a strongly textured system biased by TBs. If such a texture resulted in a high *effective* Taylor factor, it would be mimicked by the Taylor-type averaging where the overall strength is governed by the strongest orientation (for equal f_0) together with the presence of high internal stresses on the β slip systems. In the softening regime ($\lambda < 15$ nm), the effective Taylor factor could still be high, but it may be overcompensated by the dominance of the softening mechanism and the lack of sufficient internal stresses on the β slip systems leading to a pseudo-Sachs-type overall behavior. It would be worthwhile to perform further detailed analyses to check whether this hypothesis is valid.

Even with only 36 grains, the polycrystalline FE simulations of the strengthening–softening trends compare reasonably well with the experimental results, with the transition occurring at $\lambda \sim 15$ nm. Specifically, case (b) comprising all 36 grains with random orientations and distribution exhibits a relatively better corroboration with the experiments near the transition regime compared with case (a), which has only four grain orientations. As noted in the preceding paragraph, the FE polycrystalline simulations enforce conditions that are intermediate between the

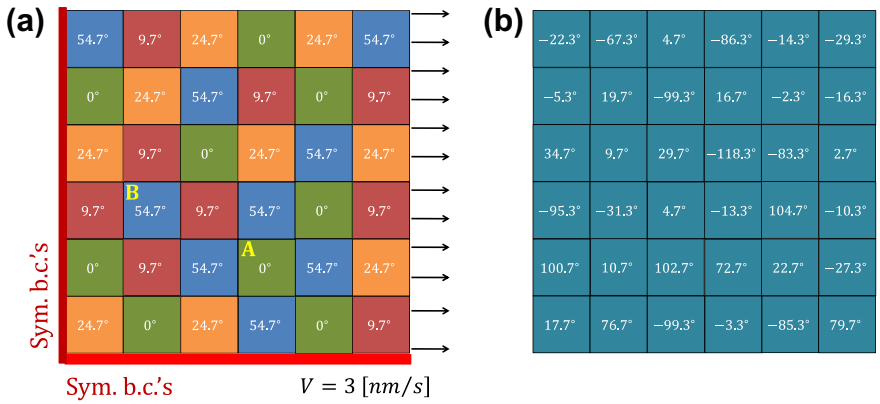

Fig. 9. Schematic representation of randomly generated 6 × 6 polycrystalline model in which (a) each grain with a given orientation appears nine times; (b) each grain has a random orientation. The TB and TBAZ within individual grains are not shown for clarity and the numbers within each grain indicate their orientation.

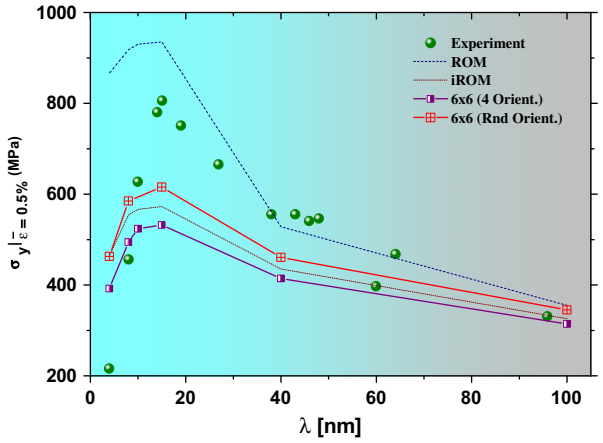

Fig. 10. Twin thickness (λ) dependent macroscopic polycrystalline yield strength (σ_y). The grain size effect has been excluded from the experimental results.

Taylor and Sachs models. Interestingly, the case (a) response is weaker than even the Sachs estimate, which indicates poor sampling of the grain orientation space in the former.

Compared with the polycrystal simulations, the experimental results show quantitatively stronger behavior for $15\ \text{nm} \leqslant \lambda \leqslant 100\ \text{nm}$ and softer behavior for $\lambda < 15\ \text{nm}$. We some light shed on the possible sources of the quantitative discrepancies. In the strengthening regime ($15\ \text{nm} \leqslant \lambda \leqslant 100\ \text{nm}$), the comparison is reasonable for the 100 nm and 40 nm cases, but the discrepancy is the largest for the 15 nm case. If one accepts that the saturation IRSS value is reasonable, given that it has some atomistic corroboration [37], the discrepancy perhaps cannot be primarily attributed to its underestimation. Therefore, such a deviation may have additional origins, and a couple of possibilities are discussed. As noted in the preceding paragraph, the discrepancy is smaller for the random grain orientation scenario (case (b)) compared with the four-grain orientation space (case (a)). This suggests that perhaps a larger grain orientation space may be necessary to obtain better corroboration, and this necessitates simulating a bigger polycrystalline matrix, which would also help from the viewpoint of the texture argument made earlier. Another possibility may be the dimensionality of the simulations, which is presently 2D-plane strain compared with a realistic 3D scenario (see for example, the differences between the 2D model of Dao et al. [12] and the 3D model of Jérusalem et al. [24]). It would be interesting to consider the 3D problem in order to better represent the influence of out-of-plane slip systems. However, neither of these extensions is trivial, as they require large computational facilities, which is currently the limitation.

In the softening regime ($\lambda < 15\ \text{nm}$), apart from the likely influence of 2D geometry, the discrepancy possibly arises from the assumption in the computational modeling that the IRSS saturates to a fixed non-zero value below λ_{cut}. From a mechanism-based argument, it may be more realistic to assume that below λ_{cut} the IRSS ceases to exist, because pile-up may become difficult or impossible, given the extremely small twin thicknesses [37]. If in the present simulations $\bar{\tau}_b^\beta = 0$ was set instead of $\bar{\tau}_b^\beta = \text{constant}$, the overall softening would be more precipitous below λ_{cut} compared with the present case. Notwithstanding this quantitative difference, an important aspect brought to the fore is that the softening mechanism may be dominant enough to prevail over the strengthening mechanism.

6.2. Micro-mechanical behavior

This section discusses the nature of plasticity that evolves within a grain inside a polycrystal and compares it with some of the characteristics discussed in Section 5.3. For easy comparison, attention is restricted to the polycrystal in Fig. 9a, and two cases are considered for a fixed twin thickness ($\lambda = 15\ \text{nm}$): (i) grain A with $\theta = 0°$ (strongest orientation) residing within the ensemble of softer grains (mainly $\theta = 54.7°$), and (ii) grain B($\theta = 54.7°$, softest grain) embedded in a sea of relatively harder grains. Fig. 11 shows the plastic slip in the polycrystal within at $\bar{\varepsilon} = 0.02$. Comparing Fig. 11 with Fig. 8c, it is interesting to note the similarity between the plastic slip concentration along and

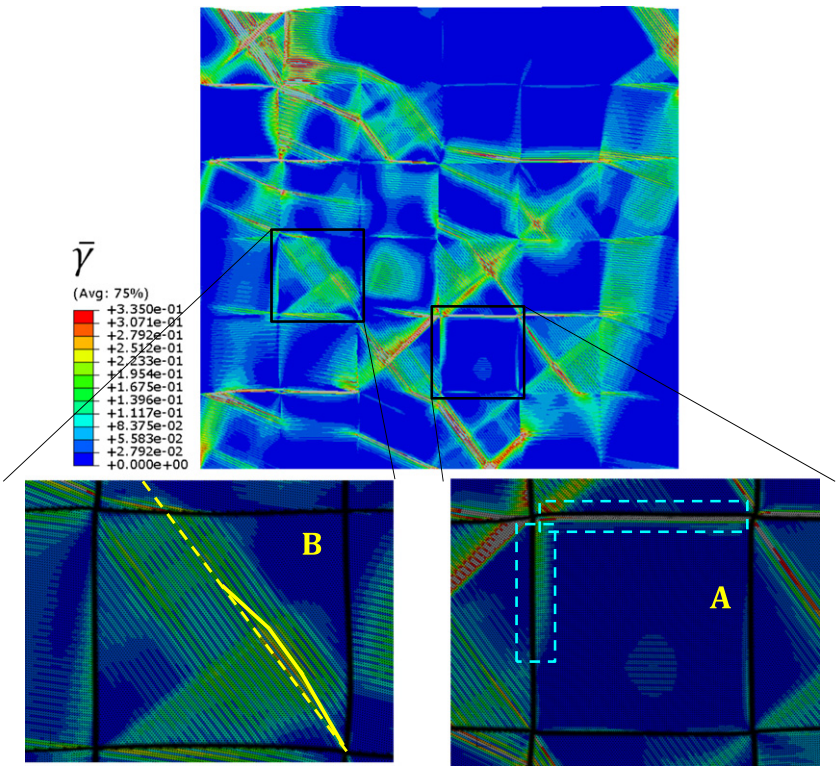

Fig. 11. The contour plot of cumulative plastic slip $\bar{\gamma}$ corresponding to the polycrystal in Fig. 9a with $\lambda = 15$ nm at $\bar{\varepsilon} = 0.02$. The enlarged view of grain B (Fig. 9a) shows the TB curvature in a soft grain ($\theta = 54.7°$) embedded within a stronger surrounding. The TB curvatures highlighted by solid yellow line, and the dashed yellow line shows its trace before deformation. In comparison, the enlarged view of a hard grain (grain A, $\theta = 0°$) embedded in softer grains shows much less plastic slip that is concentrated at the GB.

across the twin directions which extends over soft grains surrounding grain *A*. A similar situation is also observed for grain *B*, which experiences a stronger region around it. In this scenario, the plastic slip is concentrated within that grain, but the degree of localization is lower compared with its single-grain counterpart (Fig. 8c). This is primarily because the surrounding grains do not exactly mimic the strong boundary constraints imposed in the single grain model. Finally, note that in the polycrystalline setting too, the TBs experience curvature and for the same reasons explained in Section 5.3, indicating the ubiquitous nature of the phenomenon.

7. Summary and conclusions

This work developed a discrete-twin-crystal-plasticity approach that incorporates operative plasticity mechanisms in nt microstructures, with a focus on modeling the strengthening–softening yield transition in nt-Cu. The softening mechanism from profuse dislocation nucleation near TB is included as an additional plastic slip that emanates within TBAZ. Its utility in investigating macroscopic behaviors was demonstrated, while being able to resolve finer details pertaining to the manner in which microstructural plasticity is modulated within individual lamellas by its neighborhood. Based on the single grain and polycrystal simulations of nt-Cu, the findings are summarized as follows.

1. The single grain models qualitatively predict the experimentally observed macroscopic trend of a yield that exhibits strengthening with decreasing λ à la Hall–Petch behavior, but transitions to softening below a critical twin thickness.
2. The strengthening–softening response of nt-Cu stems from the competition between the anisotropic strengthening within the twin lamellas due to IRSS and the softening mediated by source-governed additional slip in the TBAZs on individual slip systems. The latter is always present in the vicinity of TB, but dominates the macroscopic response below a critical twin thickness, a combined effect of λ_z/λ ratio and decreasing CRSS within TBAZ.
3. The degree of yield strengthening and softening in a single grain is directly related to its orientation with respect to the loading direction. That is, a hard grain is macroscopically stronger and also softens less compared with a soft grain that is comparatively less strong and exhibits larger reduction in the yield strength.
4. Even if the slip systems are of non-hardening type, the macroscopic responses models may exhibit a hardening response after yield. This occurs owing to the combined effect of the anisotropy in CRSS between the α and β slip systems realized by internal stresses on the latter and the constraints applied by the surrounding medium on the GB restricting the tensile axis rotation.

5. At small twin thicknesses, the TBs also experience curvature owing to the single slip-like conditions occurring as a result of the constraints on the tensile axis rotation. Such curvatures may induce enhanced overall hardening owing to lattice incompatibilities and also mediate TB migration.
6. The polycrystal models also predict the experimental trend, albeit using a limited number of grains. The larger the grain orientation space the better is the corroboration with bulk experiments. From a different viewpoint, the results suggest that, for nt structures with only a few grains/limited orientations across the specimen dimensions, the strengthening and softening would depend on the number of grains and may not be the same as the bulk response. This aspect may be important in small-scale systems such as interconnects [37] and other systems that may employ nanoscaled structures such as nt wires, rods or thin films.
7. Although not explored here, it can be expected that the nt microstructures should exhibit increasing overall rate sensitivity with decreasing twin thickness owing to highly rate-sensitive TBAZ.

The discussion closes with remarks on the potential advantages and limitations of the current approach. The development of nt microstructures is a nascent area, and only a few homogenized models are proposed in literature (e.g. [12,24]) in the context of strengthening mechanisms. However, these approaches have not been applied to modeling the yield-softening mechanisms. The DT-CP approach seems to be an appropriate starting point to model such behavior, because it enables many of the high resolution crystallographic details prevalent in nt microstructures to be resolved. The plastic slip heterogeneities near TB that are resolved in the DT-CP approach cannot be captured by the homogenized nt models, as they smear out the discreteness. This is important, for example, in addressing the issues of ductility and modeling failure, as recent experiments show that TB spacing may affect the fracture evolution nt-Cu [10,23]. Although the homogenized models have been endowed with simple ductility criteria [12,24], a DT-CP approach may be indispensible in predicting the microstructural dependence of damage evolution [24]. It may be augmented with sophisticated techniques such as cohesive zone or XFEM approaches to model crack propagation problems. In homogenized models, lattice misorientations within individual grains have been related to TB curvatures in an average sense [12] but, as shown in this work, the DT-CP can resolve and explain the origin of the curvatures for individual TB as a function of the TB spacing, grain orientation and boundary constraints. These details must be accounted for in the homogenized models, and the DT-CP approach provides a way to probe local details. The DT-CP approach may also be naturally amenable to modeling TB migration, although such an extension is not trivial given the intricate physics of the problem. It provides a basis to probe the microstructural behavior of nt systems at length scales that are not currently accessible to MD simulations, but where discreteness matters [39,45]. Although the modeling approach is outlined for the case of nt-Cu, in principle, it should be applicable to other fcc materials that are amenable to twinning and may exhibit similar transition [46].

Unfortunately, the DT-CP approach incurs significant computational cost compared with the homogenized nt models, as it requires fine FE discretization so that the TBAZ and twin lamellas are well resolved. This is further compounded for polycrystalline models (Tables S1 and S2, Supplementary material). This limitation of the DT-CP model underscores the importance of extending homogenized approaches to account for the softening mechanisms. The DT-CP approach can be a precursor to developing such homogenized models at different levels. A first level of homogenization would be where the discreteness of lamellas may be retained, but the TBAZs may be smeared out. This would enable modeling of the heterogeneous plasticity within the lamellas, but require incorporation of the salient features of TBAZ-induced softening into the constitutive description of the parent region. One way to achieve this is to write a single constitutive law that includes a position-dependent description of the softening term (e.g. a functionally graded property). Another alternative would be to model a TB as a cohesive interface that plastic response of the TBAZ. Such an approach could also be useful in studying fracture propagation characteristics along TB. An even coarser resolution could be obtained by smearing the TB along with their TBAZ (similar to those in Dao and co-workers [12,24]). This would necessitate writing the slip constitutive laws that effectively capture the essential physics of softening. One way is to adopt volume-fraction-based averaging of the individual contributions to the overall plastic slip rate. However, the question of how to incorporate essential features pertaining to slip heterogeneity that dictate failure is not so straightforward. Our future work will focus on incorporating some of these features within the CP framework.

Acknowledgements

S.P.J. acknowledges financial support from NUS Start-up Grant R-265-000-294-133, and H.M. acknowledges support through an NUS Research Scholarship. The authors thank the anonymous reviewer for insightful comments that led to improvement of the original version of the manuscript.

Appendix A. Supplementary material

Supplementary data associated with this article can be found, in the online version, at doi:10.1016/j.actamat.2011.05.036.

References

[1] Lu L, Chen X, Huang X, Lu K. Science 2009;323:607.
[2] Li X, Wei Y, Lu L, Lu K, Gao H. Nature 2010;464:877.
[3] Ma E. JOM 2006;58:49.
[4] Chen KC, Wu WW, Liao CN, Chen LJ, Tu KN. Science 2008;321:1066.
[5] Chen M, Ma E, Hemker KJ, Sheng H, Wang Y, Cheng X. Science 2003;300:1275.
[6] Dao M, Lu L, Asaro RJ, De Hosson JTM, Ma E. Acta Mater 2007;55:4041.
[7] Gianola DS, Van Petegem S, Legros M, Brandstetter S, Van Swygenhoven H, Hemker KJ. Acta Mater 2006;54:2253.
[8] Jia D, Ramesh KT, Ma E. Acta Mater 2003;51:3495.
[9] Meyers MA, Mishra A, Benson DJ. Prog Mater Sci 2006;51:427.
[10] Shan ZW, Lu L, Minor AM, Stach EA, Mao SX. JOM 2008;60:71.
[11] Lu L, Shen Y, Chen X, Qian L, Lu K. Science 2004;304:422.
[12] Dao M, Lu L, Shen YF, Suresh S. Acta Mater 2006;54:5421.
[13] Zhu T, Li J. Prog Mater Sci 2010;55:710.
[14] Anderoglu O, Misra A, Wang J, Hoagland RG, Hirth JP, Zhang X. Int J Plast 2010;26:875.
[15] Brown JA, Ghoniem NM. Acta Mater 2009;57:4454.
[16] Brown JA, Ghoniem NM. Acta Mater 2010;58:886.
[17] Chen KC, Wu WW, Liao CN, Chen LJ, Tu KN. J Appl Phys 2010;108(066103):1.
[18] Hu Q, Li L, Ghoniem NM. Acta Mater 2009;57:4866.
[19] Kulkarni Y, Asaro RJ. Acta Mater 2009;57:4835.
[20] Wang YB, Sui ML, Ma E. Philos Mag Lett 2007;87:935.
[21] Wang YD, Liu W, Lu L, Ren Y, Nie ZH, Almer J, et al. Adv Eng Mater 2010;12:906.
[22] Wu ZX, Zhang YW, Srolovitz DJ. Acta Mater 2009;57:4508.
[23] Zhou H, Qu S, Yang W. Modell Simul Mater Sci Eng 2010:18.
[24] Jérusalem A, Dao M, Suresh S, Radovitzky R. Acta Mater 2008;56:4647.
[25] Lu K, Lu L, Suresh S. Science 2009;324:349.
[26] Shabib I, Miller RE. Acta Mater 2009;57:4364.
[27] Tschopp MA, Spearot DE, McDowell DL. Influence of grain boundary structure on dislocation nucleation in FCC metals. In: Dislocations in solids: a tribute to F.R.N. Nabarro, vol. 14. Amsterdam: Elsevier; 2008. p. 46–136 [chapter 82].
[28] Zhu T, Li J, Samanta A, Leach A, Gall K. Phys Rev Lett 2008;100:1.
[29] Jonnet J, Rémy B, Van Uffelen P. Theor Appl Fract Mech 2006;45:238.
[30] Lubarda VA, Kouris DA. Mech Mater 1996;23:191.
[31] Roy A, Peerlings RHJ, Geers MGD, Kasyanyuk Y. Mater Sci Eng A 2008;486:653.
[32] Schouwenaars R, Seefeldt M, Houtte PV. Acta Mater 2010;58:4344.
[33] Cheong KS, Busso EP, Arsenlis A. Int J Plast 2005;21:1797.
[34] Aghababaei R, Joshi SP, Reddy JN. J Mech Phys Solids 2011:59.
[35] Gurtin ME, Anand L, Lele SP. J Mech Phys Solids 2007;55:1853.
[36] Yefimov S, Groma I, Van der Giessen E. J Mech Phys Solids 2004;52:279.
[37] Zhu T, Li J, Samanta A, Kim HG, Suresh S. Proc Natl Acad Sci USA 2007;104:3031.
[38] Asaro RJ. Adv Appl Mech 1983;23:1.
[39] Wang J, Li N, Anderoglu O, Zhang X, Misra A, Huang JY, et al. Acta Mater 2010;58:2262.
[40] Peirce D, Asaro RJ, Needleman A. Acta Metall 1982;30:1087.
[41] Mesarovic SD, Baskaran R, Panchenko A. J Mech Phys Solids 2010;58:311.
[42] Needleman A, Asaro RJ, Lemonds J, Peirce D. Comput Methods Appl Mech Eng 1985;52:689.
[43] Chen XH, Lu L, Lu K. Scripta Mater 2011;64:311.
[44] Nemat-Nasser S. Plasticity: A treatise on finite deformation of heterogeneous inelastic materials – Cambridge Monographs on Mechanics. Cambridge University Press; 2009.
[45] Winther G. Mater Sci Eng A 2008;483–484:40.
[46] Stukowski A, Albe K, Farkas D. Phys Rev B – Condens Matter Mater Phys 2010:82.